Ionics (2014) 20:645–652
DOI 10.1007/s11581-013-1028-5

ORIGINAL PAPER

# Oxalate precursor preparation of $Li_{1.2}Ni_{0.13}Co_{0.13}Mn_{0.54}O_2$ for lithium ion battery positive electrode

**Chenhao Zhao · Xinxin Wang · Rui Liu · Xinru Liu · Qiang Shen**

Received: 4 July 2013 / Revised: 5 November 2013 / Accepted: 20 November 2013 / Published online: 6 December 2013


**Abstract** $Li_{1.2}Ni_{0.13}Co_{0.13}Mn_{0.54}O_2$ powders have been prepared through co-precipitation of metal oxalate precursor and subsequent solid state reaction with lithium carbonate. X-ray diffraction pattern shows that the massive rock-like structure has a good layered structure and solid solution characteristic. Scanning electron microscope and transition electron microscope images reveal that the $Li_{1.2}Ni_{0.13}Co_{0.13}Mn_{0.54}O_2$ composed of nanoparticles have the size of 1–2 μm. As a lithium ion battery positive electrode, the $Li_{1.2}Ni_{0.13}Co_{0.13}Mn_{0.54}O_2$ has an initial discharge capacity of 285.2 mAh $g^{-1}$ at 0.1 C within 2.0–4.8 V. When the cutoff voltage is decreased to 4.6 V, the cycling stability of product can be greatly improved, and a discharge capacity of 178.5 mAh $g^{-1}$ could be retained at 0.5 C after 100 cycles. At a high charge–discharge rate of 5 C (1,000 mAh $g^{-1}$), a stable discharge capacity of 121.4 mAh $g^{-1}$ also can be reached. As the experimental results, the $Li_{1.2}Ni_{0.13}Co_{0.13}Mn_{0.54}O_2$ prepared from oxalate precursor route is suitable as lithium ion battery positive electrode.

**Keywords** Oxalate precursor · $Li_{1.2}Ni_{0.13}Co_{0.13}Mn_{0.54}O_2$ · Positive electrode · Cutoff voltage

## Introduction

Development of positive electrode materials with high capacity, long cycle life, and low cost has been one of the most important subjects for high-performance lithium ion batteries [1, 2]. Recently, the lithium-rich manganese-based oxides $xLi_2MnO_3 \cdot (1\text{-}x)LiMO_2$ (M = Ni, Co, Mn, Fe, Cr, $Ni_{1/2}Mn_{1/2}$, $Ni_{1/3}Co_{1/3}Mn_{1/3}$…) have received many attentions due to their high reversible capacity (230–300 mAh $g^{-1}$) [3–8]. As for a solid solution electrode, the $Li_2MnO_3$ component is considered to stabilize the crystal structure and enhance the discharge capacity through extracting the lithium ions concomitant with release of oxygen at charge voltage within 4.5–4.6 V, to form an active $MnO_2$ component. Therefore, the solid solutions could reach special high capacity and retain good cycling stability upon cycling [3–11].

$Li_{1.2}Ni_{0.13}Co_{0.13}Mn_{0.54}O_2$ (or described as $0.5Li_2MnO_3$ $0.5LiNi_{1/3}Co_{1/3}Mn_{1/3}O_2$) stands out from other solid solution materials due to its high discharge capacity, moderate cycling performance, and good rate capability. Therein, the *C2/m* $Li_2MnO_3$ can well integrate with equivalent *R-3m* $LiNi_{1/3}Co_{1/3}Mn_{1/3}O_2$ [4–6], and the improved electrochemical performances of $Li_{1.2}Ni_{0.13}Co_{0.13}Mn_{0.54}O_2$ should be ascribed to the good synergistic effect of $Li_2MnO_3$ and $LiNi_{1/3}Co_{1/3}Mn_{1/3}O_2$ components and the appropriate existence of cobalt [12–15]. As the experimental results, the initial discharge capacity of $Li_{1.2}Ni_{0.13}Co_{0.13}Mn_{0.54}O_2$ can reach as high as 260–310 mAh $g^{-1}$ at low current density, and its capacity retention also reaches 70~90 % after a dozen or even a hundred cycles [16–21]. Conventional inorganic preparation methods such as sol–gel [16, 20], solid state [22], sucrose combustion [16], molten salt [17], and polymer gel [23] have been successfully introduced to prepare the good solid solution material, showing the structural and electrochemical properties of $Li_{1.2}Ni_{0.13}Co_{0.13}Mn_{0.54}O_2$ which are determined by the synthesis methods and preparation conditions [19].

Recently, the preparation technologies through initial co-precipitation and subsequent solid state reaction have become one of the most promising routes to synthesize multiple oxides such as $Li_xNi_yCo_zMn_{2\text{-}x\text{-}y\text{-}z}O_2$ [15, 18, 24, 25]. The $Li_{1.2}Ni_{0.13}Co_{0.13}Mn_{0.54}O_2$ with controlled morphologies and sizes also can be readily obtained by using suitable multiple

C. Zhao · X. Wang · R. Liu · X. Liu · Q. Shen (✉)
Key Laboratory for Colloid and Interface Chemistry of Education Ministry, School of Chemistry and Chemical Engineering, Shandong University, Jinan 250100, China
e-mail: qshen@sdu.edu.cn

metal salts templates such as $Ni_{0.13}Co_{0.13}Mn_{0.54}(OH)_{1.6}$ [18] and $Ni_{0.13}Co_{0.13}Mn_{0.54}(CO_3)_{0.8}$ [25]. In the present study, the mixed synthesis route including initial co-precipitation of metal oxalate precursor and subsequent solid state reaction with lithium carbonate is used to prepare $Li_{1.2}Ni_{0.13}Co_{0.13}Mn_{0.54}O_2$. The purpose of the mixed oxalate route is to produce micro-size $Li_{1.2}Ni_{0.13}Co_{0.13}Mn_{0.54}O_2$ composed of nanoparticles [25]. Correspondingly, the structures, morphologies, and electrochemical performances of $Li_{1.2}Ni_{0.13}Co_{0.13}Mn_{0.54}O_2$ particles are also discussed in the text.

## Experimental

### Synthesis of $Li_{1.2}Ni_{0.13}Co_{0.13}Mn_{0.54}O_2$

First, 1.39 g of $Mn(AC)_2{\cdot}4H_2O$, 0.34 g of $Co(AC)_2{\cdot}4H_2O$ and 0.34 g of $Ni(AC)_2{\cdot}4H_2O$ were dissolved into 40-mL equal volume mixed solution of water and ethanol, and then 40 mL of the same water and ethanol mixed solution containing 1.52 g $H_2C_2O_4{\cdot}2H_2O$ was added drop by drop under stirring. The obtained suspension was transferred into a 100-mL teflon-lined autoclave, and kept at 80 °C for 5 h. The precipitated metal oxalate was filtered, washed thoroughly with ultra-pure water and ethanol, and then dried at 80 °C for 5 h. Then, 0.6 g freshly prepared metal oxalate was mixed well with 0.1844 g $Li_2CO_3$ (3 % excess) in an agate mortar using ethanol as dispersant. The obtained mixture was pre-calcined at 450 °C for 4 h, calcined at 850 °C for 12 h, and cooled naturally to room temperature.

### Crystal characterization

Thermogravimetric analysis (TGA) and differential scanning calorimetry (DSC) measurements were carried out on a Mettler (SDTQ-600) to monitor the weight loss and heat flow of metal oxalate precursor and metal oxalate-$Li_2CO_3$ mixture at heating rate of 10 °C $min^{-1}$ from room temperature to 800 or 900 °C under an air atmosphere. X-ray diffractometer (XRD) patterns of 80 °C-treated hydrothermal precursor, corresponding to $Li_{1.2}Ni_{0.13}Co_{0.13}Mn_{0.54}O_2$ and cycled product were collected on a Rigaku D/max-2400 powder XRD, (0.08 ° pot/s). SEM (JEOL JSM-7600F, 5 kV) and TEM (JEM-100CX11, 100 kV) were conducted to characterize the morphologies and sizes of precursor metal oxalate and product $Li_{1.2}Ni_{0.13}Co_{0.13}Mn_{0.54}O_2$.

### Electrochemical characterization

CR 2032 coin cells of $Li_{1.2}Ni_{0.13}Co_{0.13}Mn_{0.54}O_2$/Li were used for electrochemical experiments performed at room temperature. The working electrodes were prepared as the following: after mixing of electrode materials, acetylene black and poly(vinyl difluoride) at a weight ratio of 80:10:10, the resulting mixtures were slurried with N-methyl-2-pyrrolidone, pasted onto aluminum foils, dried at 80 °C for 5 h, and cut into disks with a diameter of 12 mm with a positive electrode material loading density of 2.62±0.35 mg $cm^{-2}$. Glass fibers (Whatman) were used as separators, and the electrolyte (LBC 305–01, Shenzhen Xinzhoubang) is the $LiPF_6$ in EC, EMC, and DMC-mixed solvent. The cells were assembled in an argon-filled glove box. Galvanostatic cycling tests were conducted on a Land CT2001A battery system at various current rates (1 C= 200 mAh $g^{-1}$) within 2.0–4.6 and 2.0–4.8 V. After the 100-cycle tests, parts of the lithium ion batteries were unpacked in an air–atmosphere ventilating cabinet, therein the active materials of the working electrodes were washed with acetone and then ethanol three times, dried at 80 °C, and then used for tests.

## Results and discussion

Figure 1 shows the TGA-DSC curves of metal oxalate precursor and metal oxalate-$Li_2CO_3$ mixture from room temperature to 800 or 900 °C at a heating rate of 10 °C $min^{-1}$. In Fig. 1a, the first weight loss of ca. 20 wt.% from room temperature to 250 °C with broad endothermic peak in DSC curve would be related with dehydration of metal oxalate, and the weight loss is close to the value of 19.9 wt.%, which is calculated from the dehydration of $Ni_{0.13}Co_{0.13}Mn_{0.54}(C_2O_4)_{0.8}{\cdot}1.6H_2O$. When the temperature is increased above 300 °C, the anhydrous metal oxalate is decomposed into metal oxide and carbon dioxide accompanied with the release of heat. In Fig. 1b, the weight loss before 300 °C should be the dehydration and decomposition of metal oxalate [26, 27]. After that, a weak exothermic peak nearby 400 °C may be attributed to the beginning of crystallization of target product $Li_{1.2}Ni_{0.13}Co_{0.13}Mn_{0.54}O_2$ [26]. Furthermore, From the TGA profile, the mass loss is almost stopped until 800 °C, indicating that the crystallization temperature of $Li_{1.2}Co_{0.13}Ni_{0.13}Mn_{0.54}O_2$ should be above 800 °C, and the total weight loss of metal oxalate-$Li_2CO_3$ mixture is 55.6 % from room temperature to 900 °C, which agree well with the theoretical data of 54.9 % according to the total chemical reaction:

$$Ni_{0.13}Co_{0.13}Mn_{0.54}(C_2O_4)_{0.8}{\cdot}1.6H_2O + 0.6Li_2CO_3 + 0.7O_2 \rightarrow Li_{1.2}Ni_{0.13}Co_{0.13}Mn_{0.54}O_2 + 1.6H_2O\uparrow + 2.2CO_2\uparrow$$

According to the TGA-DSC results in Fig. 1b and early papers on calcination temperature [19, 22, 23], the mixture is decomposed at 450 °C for 4 h and crystallization treatment at 850 °C for 12 h to obtain the target product.

The XRD patterns of precursor $Ni_{0.13}Co_{0.13}Mn_{0.54}(C_2O_4)_{0.8}{\cdot}1.6H_2O$ and product $Li_{1.2}Ni_{0.13}Co_{0.13}Mn_{0.54}O_2$ are revealed in Fig. 2. The diffraction peaks of precursor in Fig. 2a can be indexed to monoclinic structure $MnC_2O_4{\cdot}2H_2O$

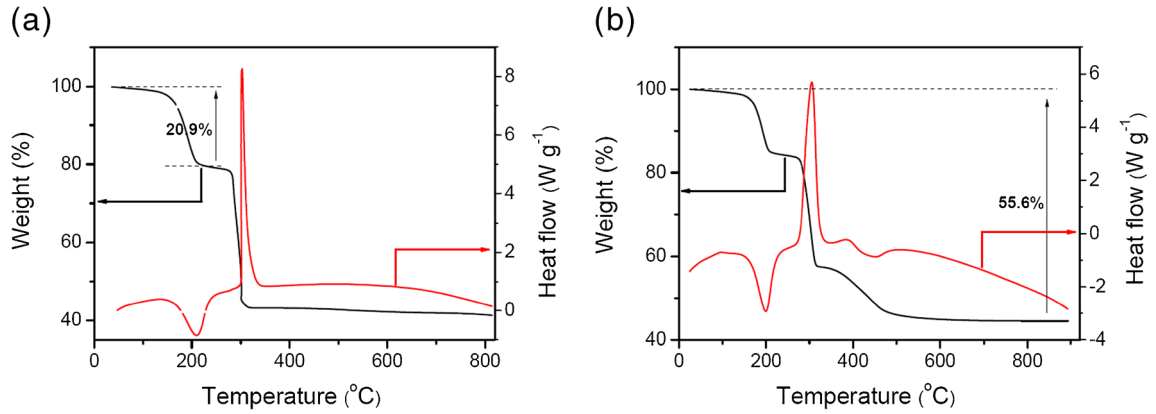


**Fig. 1** TGA-DSC analysis of metal oxalate precursor (**a**) and metal oxalate-$Li_2CO_3$ mixture (**b**) from room temperature to 800 or 900 °C at a heating rate of 10 °C min$^{-1}$

(JCPDS: 25–0544) [27, 28]. The further calcination of metal oxalate with $Li_2CO_3$ at 850 °C results in the formation of $Li_{1.2}Co_{0.13}Ni_{0.13}Mn_{0.54}O_2$, and the corresponding XRD pattern with the Miller indices is showed in Fig. 2b. All of the diffraction peaks can be attributed to hexagonal layered structure with space group of $R\,\bar{3}\,m$ except the weak diffraction peaks marked by asterisk. In fact, the $Li_2MnO_3$ component in a solid solution can also be referred to as the $LiMO_2$ (i.e., $M^{3+} = Li^{+}_{1/3}Mn^{4+}_{2/3}$) formula, meaning that tetravalent manganese and monovalent lithium construct the trivalent M layer in $LiMO_2$ lattice structures. Especially, the alternating arrangement of $Li^+$ and $Mn^{4+}$ ions in the $Li^{+}_{1/3}Mn^{4+}_{2/3}$ layer may induce the appearance of XRD superlattice signals. The asterisk-marked weak diffraction peaks correspond to the XRD characteristics of $LiMO_2$ superlattice structures within the $2\theta$ range of 20 and 25°, indicating the coexistence of crystalline $Li_2MnO_3$ phase in solid solution [12–15]. Also, the strong and sharp diffraction peaks of Fig. 2b indicate a good crystallinity of products.

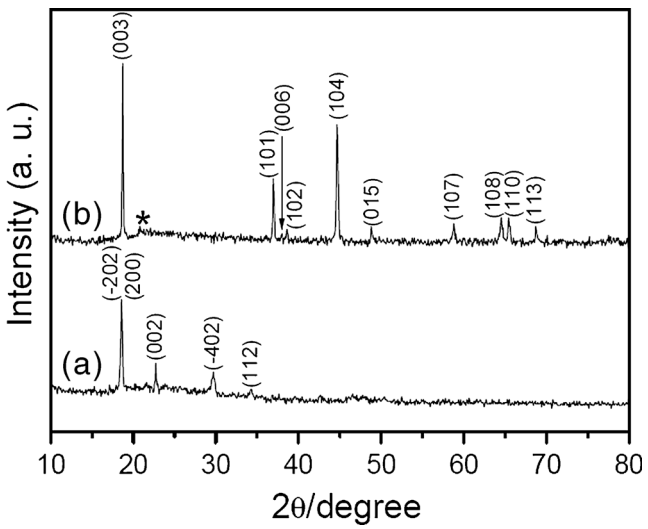


**Fig. 2** XRD patterns of precursor $Ni_{0.13}Co_{0.13}Mn_{0.54}(C_2O_4)_{0.8}\cdot 1.6H_2O$ (**a**) and resulting $Li_{1.2}Ni_{0.13}Co_{0.13}Mn_{0.54}O_2$ (**b**)

Table 1 reveals lattice parameters, the ratios of $I_{(003)}/I_{(104)}$ and the estimated crystallite size for $Li_{1.2}Ni_{0.13}Co_{0.13}Mn_{0.54}O_2$ samples calculated from the XRD data using the $R\,\bar{3}\,m$ space group. The calculated lattice parameters are closed to the layered $LiNi_{1/3}Co_{1/3}Mn_{1/3}O_2$ [29]. As we know, the integrated intensity ratio of the (003) to (104) peak ($I_{(003)}/I_{(104)}$) in XRD pattern can be used as a measurement of layered structure and cation mixing, and a value greater than 1.2 is an indication of good layered structure and low cation mixing. Herein, the $I_{(003)}/I_{(104)}$ of as-prepared $Li_{1.2}Co_{0.13}Ni_{0.13}Mn_{0.54}O_2$ can reach 1.49, indicating the material has good layered structure, which also can be further confirmed by well peaks splits of (006)/(102) and (108)/(110) diffraction peaks [30, 31].

The morphologies and surface structures of precursor $Ni_{0.13}Co_{0.13}Mn_{0.54}(C_2O_4)_{0.8}\cdot 1.6H_2O$ and product $Li_{1.2}Ni_{0.13}Co_{0.13}Mn_{0.54}O_2$ are shown in Fig. 3. The micro-size precursor has the size of 1–2 μm, and its particle surface is very smooth in Fig. 3a, b. Interestingly, some terrace-like structures can be observed for a single oxalate particle, which may be attributed to special nucleation habit of metal oxalate comparing with other precipitations such as metal carbonates and metal hydroxides [16, 18, 25]. As we expected, the morphology of precursor can be partially maintained after calcination with $Li_2CO_3$ at high temperature in Fig. 3c. The particles size of resulting $Li_{1.2}Ni_{0.13}Co_{0.13}Mn_{0.54}O_2$ is slightly smaller than that of precursor and the average diagonal length decrease from 1.53 to 1.38 μm after calcination. From the enlarged particle picture in Fig. 3d, it can be found that the $Li_{1.2}Ni_{0.13}Co_{0.13}Mn_{0.54}O_2$ is aggregated by nanoparticles. Figure 4 reveals the TEM image of the edge of a single

**Table 1** Lattice parameters, the ratios of $I_{(003)}/I_{(104)}$ and the estimated crystallite size for $Li_{1.2}Ni_{0.13}Co_{0.13}Mn_{0.54}O_2$ samples calculated from the XRD data using the $R\,\bar{3}\,m$ space group

| a (Å) | c (Å) | c/a | $I_{(003)}/I_{(104)}$ | Crystallite size (nm) |
|---|---|---|---|---|
| 2.848 | 14.221 | 4.993 | 1.49 | 57.29 |

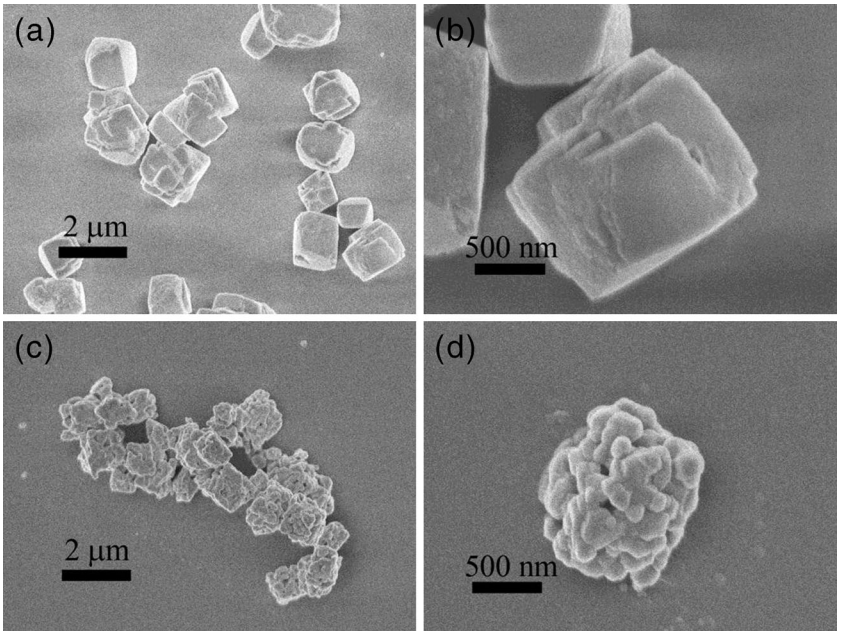


**Fig. 3** SEM images of precursor $Ni_{0.13}Co_{0.13}Mn_{0.54}(C_2O_4)_{0.8}{\cdot}1.6H_2O$ (**a**, **b**) and resulting $Li_{1.2}Ni_{0.13}Co_{0.13}Mn_{0.54}O_2$ (**c**, **d**)

$Li_{1.2}Ni_{0.13}Co_{0.13}Mn_{0.54}O_2$ particle. Some nanoparticles with a sharp corner and edge can be found in the picture. These nanoparticles have the size of 60–150 nm, which is a little larger than the estimated crystallite size (about 57 nm) based on full width at half maximum of (003) crystal plane and Sheerer equation ($D = k\lambda/B\cos\theta$) in Table 1.

Figure 5 shows the energy-dispersive x-ray spectroscopy (EDS) spectrum of $Li_{1.2}Ni_{0.13}Co_{0.13}Mn_{0.54}O_2$ prepared from oxalate precursor route. The estimated element ratio of Ni/Co/Mn is 0.12(4):0.13(0):0.58 (1). Considering the allowable error (±10 %) of the EDS result, the measured nanoparticle is approximately homogeneous in chemical composition as that of solid solution $Li_{1.2}Ni_{0.13}Co_{0.13}Mn_{0.54}O_2$.

Based on the above results, the formation process of $Li_{1.2}Ni_{0.13}Co_{0.13}Mn_{0.54}O_2$ can be described as follows: in the first step, after adding precipitant oxalic acid into mixed metal salts solution, the nucleation and crystal growth of metal oxalate will start, and the precursor can be obtained. In the next step, the oxalate precursor plays a role as sacrificed template on the formation of $Li_{1.2}Ni_{0.13}Co_{0.13}Mn_{0.54}O_2$, and the structure composed of nanoparticles can be produced due to the generation of carbon dioxide and vapor. As an experimental result, the well-defined nanoparticles can provide a solid framework during the intercalation/decalation of lithium ions. Also, these nanoparticles can shorten the diffusion route of lithium ions and electrons, especially for lithium-rich manganese-based oxides, which have lower electrochemical conductivity [16, 19, 32].

The initial charge discharge profiles of $Li_{1.2}Ni_{0.13}Co_{0.13}Mn_{0.54}O_2$ at 0.1C (20 mA $g^{-1}$) within 2.0–4.6 and 2.0–4.8 V are shown in Fig. 6a. During the charging at the potential below 4.4 V, the capacity can be ascribed to deintercalation of Li ions accompanied by the oxidation of $Ni^{2+}$ ions within $LiNi_xCo_yMn_{1-x-y}O_2$ component [14, 31]. The plateau nearby 4.5–4.6 V corresponds to both the loss of $Li_2O$ from $Li_2MnO_3$ phases and the oxidation of $Co^{3+}$ ions within

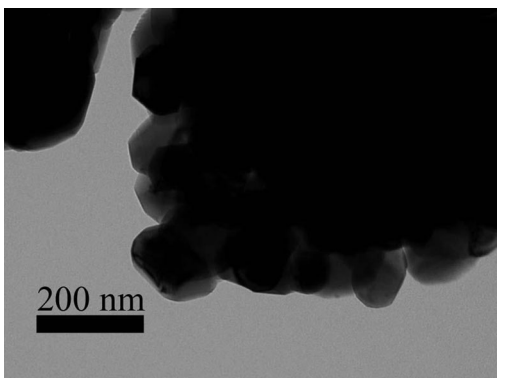


**Fig. 4** TEM image of the edge of single $Li_{1.2}Ni_{0.13}Co_{0.13}Mn_{0.54}O_2$ particle

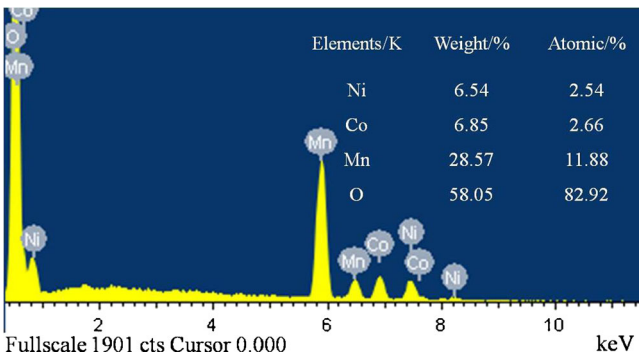


**Fig. 5** EDS analysis of $Li_{1.2}Ni_{0.13}Co_{0.13}Mn_{0.54}O_2$

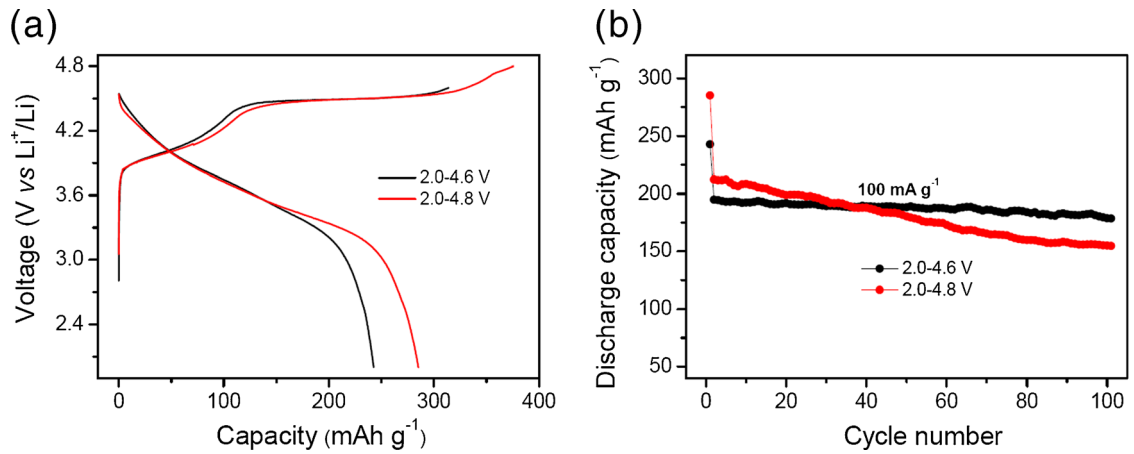


**Fig. 6** Initial charge discharge profiles at 0.1 °C (**a**) and cycling performances (**b**) of $Li_{1.2}Ni_{0.13}Co_{0.13}Mn_{0.54}O_2$ within 2.0–4.6 and 2.0–4.8 V

active $LiNi_xCo_yMn_{1-x-y}O_2$ components. In the discharge profile, the corresponding 4.5-V plateau cannot be found, indicating that the $Li_2MnO_3$ would not be recovered and irreversible $Li_2MnO_3 \rightarrow MnO_2 \rightarrow LiMnO_2$ transformation accounts for the high-capacity feature of solid solution material [3–15]. The discharge capacity and coulombic efficiency of $Li_{1.2}Ni_{0.13}Co_{0.13}Mn_{0.54}O_2$ can be partially determined by cutoff voltage. At the voltage window of 2.0–4.6 V, a discharge capacity of 242.7 mAh $g^{-1}$ with coulombic efficiency of 77.6 % can be obtained. When the cutoff voltage is elevated to 4.8 V, the discharge capacity increases to 285.2 mAh $g^{-1}$, and the coulombic efficiency decreases to 75.8 %.

After the initially preset one charge–discharge cycle at 0.1 C the electrochemical cycling stability of $Li_{1.2}Ni_{0.13}Co_{0.13}Mn_{0.54}O_2$ is measured at 0.5 C for the subsequent 100 cycles. As shown in Fig. 6b, when the cutoff voltage is set as 4.6 V, the second cycle discharge capacity is194.8 mAh $g^{-1}$, over the 100 cycles; the residual value is 178.5 mAh $g^{-1}$. Briefly, high capacity (178.5 mAh $g^{-1}$) and capacity retention (91.6 %) after 100 cycles can be obtained for $Li_{1.2}Ni_{0.13}Co_{0.13}Mn_{0.54}O_2$. However, when the cutoff voltage increases to 4.8 V, the discharge capacity of $Li_{1.2}Ni_{0.13}Co_{0.13}Mn_{0.54}O_2$ quickly drops from 212.3 (second cycle) to 154.7 mAh $g^{-1}$(100th cycle). According to the above results, a low cutoff voltage (i.e., 4.6 V) is more suitable for the electrochemical cycling purpose. Simultaneously, a summary for the electrochemical performances of $Li_{1.2}Ni_{0.13}Co_{0.13}Mn_{0.54}O_2$ obtained from different preparation routes and conditions is revealed in Table 2; by comparison, the electrochemical performances especially cycling stability of $Li_{1.2}Ni_{0.13}Co_{0.13}Mn_{0.54}O_2$ are not poor.

In order to further study the electrochemical and structural changes at different cutoff voltages, typical 2nd, 10th, 50th, and 100th charge discharge curves and corresponding dQ/dV profiles of $Li_{1.2}Ni_{0.13}Co_{0.13}Mn_{0.54}O_2$ are revealed in Fig. 7. The solid solution material experiences voltage decay from the 2nd to the 101st cycle marked by arrow in Fig. 7a, c. Three pairs of redox peaks including layered $Co^{4+}/Co^{3+}$, $Ni^{4+}/Ni^{2+}$, and spinel $Mn^{4+}/Mn^{3+}$ can be observed in dQ/dV profiles as shown in Fig. 7b. Interestingly, as the cycles increase, the cathodic peak of layered $Ni^{4+}/Ni^{2+}$ nearby 3.8 V weaken gradually, and the cathodic peak of spinel $Mn^{4+}/Mn^{3+}$ nearby 3.0 V becomes stronger, meaning that the layered structure of solid solution is partially transformed into spinel structure during cycling [19]. In Fig. 7d, the structural phase transformation is more serious, and the serious transformation can account for the poor cycling stability when operating at the voltage window of 2.0–4.8 V. Figure 8 reveals the XRD patterns of $Li_{1.2}Ni_{0.13}Co_{0.13}Mn_{0.54}O_2$

**Table 2** Summary of the electrochemical performances of $Li_{1.2}Ni_{0.13}Co_{0.13}Mn_{0.54}O_2$ obtained from different preparation routes and conditions

| Routes | Morphologies and size or structures | Initial capacity (mAh $g^{-1}$) | Capacity retention | Ref. |
|---|---|---|---|---|
| Oxalate precursor | Massive rock-like/1–2 μm | 285.2 | 91.6 %/100 cycles* | This work |
| Sol–gel | Nanoparticles/0.2–0.4 μm | 262.5 | 74.0 %/60 cycles | [16] |
| Molten salt | Nanoparticles/~0.1 μm | 313.0 | ~70 %/100 cycles | [17] |
| Fast co-precipitation | Nanoparticles/0.2–0.5 μm | 315.3 | <77.6 %/30 cycles | [18] |
| Tartaric acid assist | Nanoparticles/0.2–0.5 μm | 281.1 | ~70 %/50 cycles | [19] |
| Precipitation | $FePO_4$ coated | 271.7 | 84.9 %/100 cycles | [20] |
| Mixing | Graphene wrapped | ~290 | ~90 %/100 cycles | [21] |

*: Data are based on cutoff voltage 4.6 V

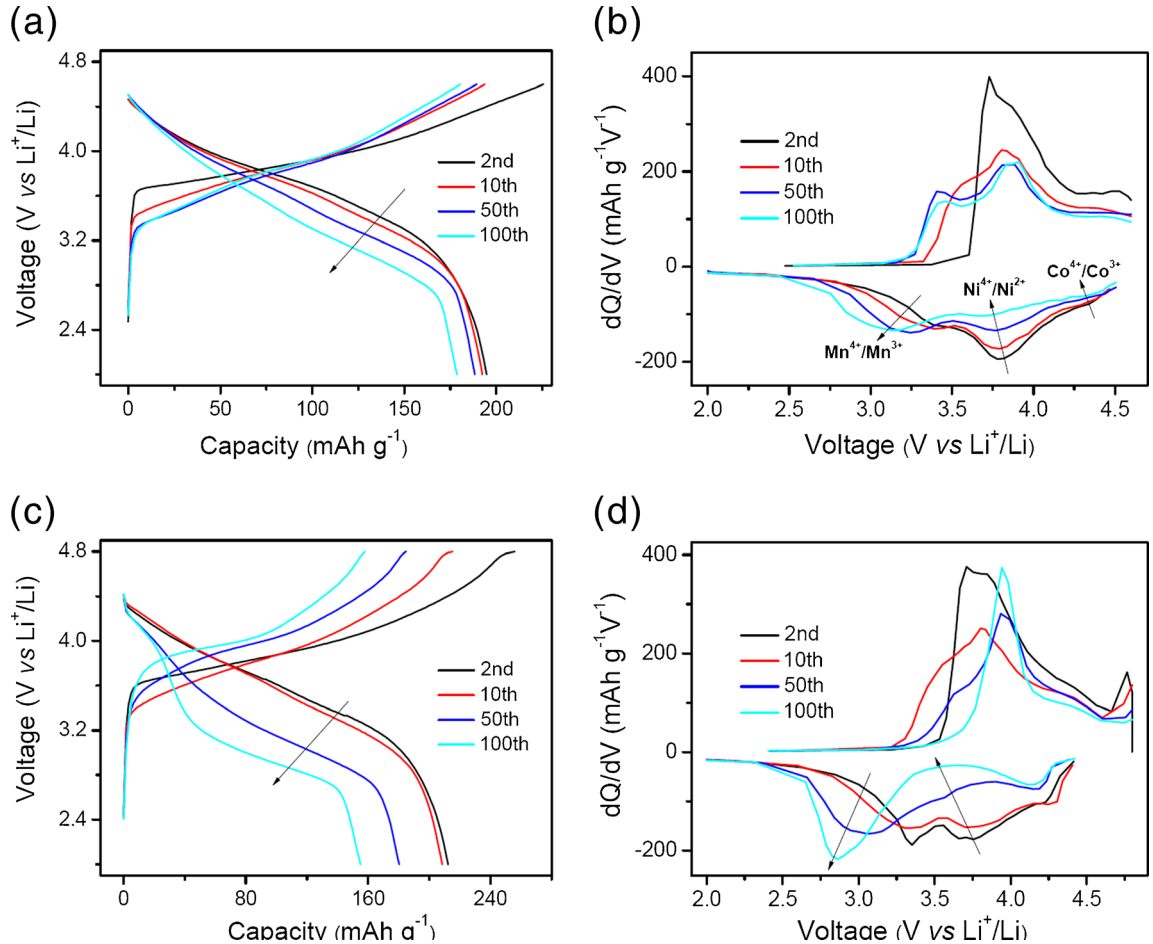


**Fig. 7** Typical 2nd, 10th, 50th, and 100th charge discharge curves and corresponding dQ/dV profiles of $Li_{1.2}Ni_{0.13}Co_{0.13}Mn_{0.54}O_2$ at 0.5 °C within 2.0–4.6 V (**a**, **b**) and 2.0–4.8 V (**c**, **d**)

cycled after 100 cycles within 2.0–4.6 and 2.0–4.8 V. The peak intensity of 4.6 V cycled product is stronger than that of 4.8 V cycled product. Also, the value of $I_{(003)}/I_{(104)}$ decreases from 1.18 to 1.11 when the cutoff voltage increases from 4.6 to 4.8 V. These results suggest that the layered structure can be better retained at low cutoff, which delect is consistent with the result in Fig. 7.

The rate capability of $Li_{1.2}Ni_{0.13}Co_{0.13}Mn_{0.54}O_2$ was also evaluated at different current densities and cutoff voltages as

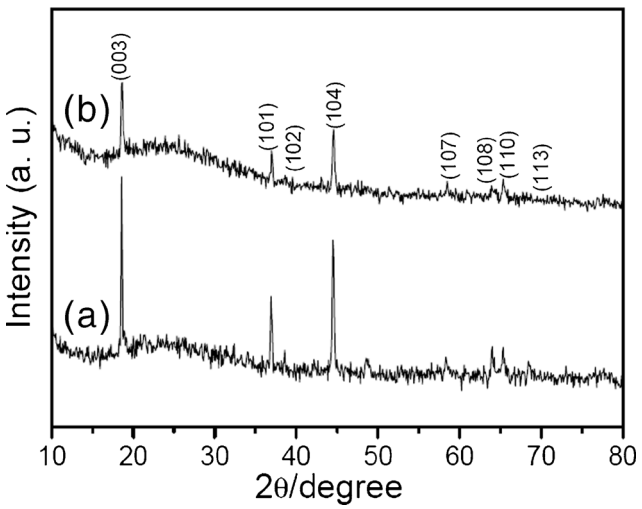


**Fig. 8** XRD patterns of $Li_{1.2}Ni_{0.13}Co_{0.13}Mn_{0.54}O_2$ cycled after 100 cycles within 2.0–4.6 (**a**) and 2.0–4.8 V (**b**)

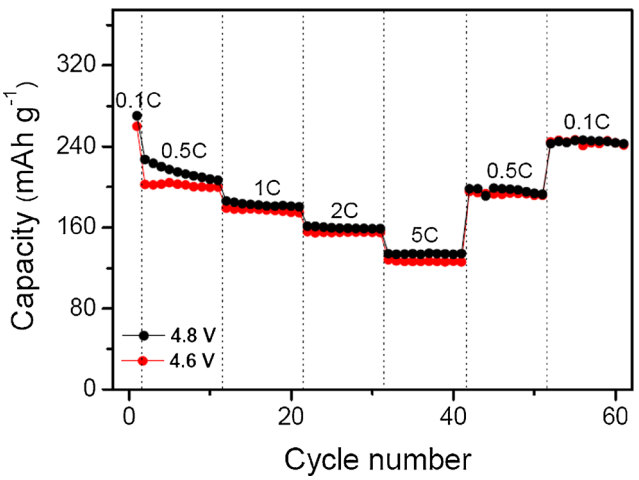


**Fig. 9** Rate capability of $Li_{1.2}Ni_{0.13}Co_{0.13}Mn_{0.54}O_2$ evaluated at different current densities within 2.0–4.6 and 2.0–4.8 V

shown in Fig. 9. It is found that the rate capability performance is less affected by the different cutoff voltages in comparison with cycling stability. When 4.6 V is selected as the cutoff voltage, the 22nd specific discharge capacity of $Li_{1.2}Ni_{0.13}Co_{0.13}Mn_{0.54}O_2$ is 155.8 mAh $g^{-1}$ at 2 C and the 32nd reversible capacity at 5 C still keeps at a value of 128.3 mAh $g^{-1}$. More importantly, when the current density goes back to 0.1 C, the 52nd cycle discharge capacity returns to a high value of 246.1 mAh $g^{-1}$, which is 94.6 % of the initial discharge capacity at 0.1 C. These indicate that the $Li_{1.2}Ni_{0.13}Co_{0.13}Mn_{0.54}O_2$, as a positive electrode material, could be a promising candidate for lithium ion batteries with good rate capacity.

## Conclusion

In summary, the two-step preparation route including initial oxalate co-precipitation and subsequent solid state reaction with lithium carbonate is used to prepare high-capacity positive electrode material $Li_{1.2}Ni_{0.13}Co_{0.13}Mn_{0.54}O_2$. The structural measurements reveal that, the $Li_{1.2}Ni_{0.13}Co_{0.13}Mn_{0.54}O_2$ composed of nanoparticles has a good layered structure. As a lithium ion battery positive material, the $Li_{1.2}Ni_{0.13}Co_{0.13}Mn_{0.54}O_2$ shows good cycling stability and rate capability at the electrochemical window of 2.0–4.6 V. According to the above results, the good lithium storage ability of $Li_{1.2}Ni_{0.13}Co_{0.13}Mn_{0.54}O_2$ may be attributed to its ordered layered structure and special morphology.

**Acknowledgment** The authors thank the financial supports from Shandong Province (ZR2012BM001), from the National Basic Research Program of China (2011CB935900) and from the NCET Program in the University.

## References

1. Ellis BL, Lee KT, Nazar LF (2010) Positive electrode materials for Li-ion and Li-batteries. Chem Mater 22:691–714
2. Goodenough JB, Kim YS (2010) Challenges for rechargeable Li batteries. Chem Mater 22:587–603
3. He P, Yu HJ, Zhou HS (2012) Layered lithium transition metal oxide cathode towards high energy lithium-ion batteries. J Mater Chem 22: 3680–3695
4. Yu HJ, Zhou HS (2013) High-energy cathode materials ($Li_2MnO_3$-$LiMO_2$) lithium-ion batteries. J Phys Chem Lett 4:1268–1280
5. Thackeray MM, Johnson CS, Vaughey JT, Li N, Hackney SA (2005) Advances in manganese-oxide 'composite' electrodes for lithium ion batteries. J Mater Chem 15:2257–2267
6. Thackeray MM, Kang SH, Johnson CS, Vaughey JT, Benedek R, Hackney SA (2007) $Li_2MnO_3$-stabilized $LiMO_2$ (M=Mn, Ni, Co) electrodes for lithium ion batteries. J Mater Chem 17:3112–3125
7. Liu YJ, Liu SB (2013) Effect of cooling method on the electrochemical performance of $0.5Li_2MnO_3{\cdot}0.5LiNi_{0.5}Mn_{0.5}O_2$ cathodes. Ionics 19:477–481
8. Shi YF, Liu H, Liu GB, You XW (2013) The preparation and electrochemical properties of the Li-excess cathode material $Li_{1+x}(Mn_{0.7}Fe_{0.3})_{1-x}O_2$ by coprecipitation method. Ionics DOI: 10.1007/s11581-013-0900-7
9. Lin J, Mu DB, Yin J, Wu BR, Ma YF, Wu F (2013) Li-rich layered composite $Li[Li_{0.2}Ni_{0.2}Mn_{0.6}]O_2$ synthesized by a novel approach as cathode material for lithium ion battery. J Power Sources 230:76–80
10. Xiang XD, Li XQ, Li WS (2013) Preparation and characterization of size-uniform $Li[Li_{0.131}Ni_{0.304}Mn_{0.565}]O_2$ particles as cathode materials for high energy lithium ion battery. J Power Sources 230:89–95
11. Yu C, Guan XF, Li GS, Zheng J, Li LP (2012) A novel approach to composite electrode $0.5Li_2MnO_3{\cdot}0.5LiNi_{0.5}Mn_{0.5}O_2$ in lithium-ion batteries with an anomalous capacity and cycling stability at 45.4 °C. Scr Mater 66:300–303
12. Guo XJ, Li YX, Zheng M, Zheng JM, Li J, Gong ZL, Yang Y (2008) Structural and electrochemical characterization of $xLi[Li_{1/3}Mn_{2/3}]O_2{\cdot}(1\text{-}x)Li[Ni_{1/3}Co_{1/3}Mn_{1/3}]O_2$ ($0\le x\le 0.9$) as cathode materials for lithium ion batteries. J Power Sources 184:414–419
13. Johnson CS, Li NC, Lefief C, Vaughey JT, Thackeray MM (2008) Synthesis, characterization and electrochemistry of lithium batteries electrodes $xLiMnO_3{\cdot}(1\text{-}x)LiNi_{0.333}Co_{0.333}Mn_{0.333}O_2$ ($0\le x\le 0.7$). Chem Mater 20:6095–6106
14. Zhao CH, Kang WP, Liu R, Shen Q (2013) Influence of cobalt on the electrochemical properties of sheet-like $0.5Li_2MnO_3{\cdot}0.5LiNi_{1/3+x}Co_{1/3-2x}Mn_{1/3+x}O_2$ as lithium ion battery cathodes. RSC Adv 2: 2362–2368
15. Liu FL, Zhang S, Deng C, Wu Q, Zhang M, Meng FL, Gao H, Sun YH (2012) Cobalt content optimization of layered $0.6Li[Li_{1/3}Mn_{2/3}]O_2$–$0.4LiNi_{0.5-x}Mn_{0.5-x}Co_{2x}O_2$ ($0\le x\le 0.5$) cathode materials prepared by the carbonate coprecipitation. J Electrochem Soc 159: A1591–A1597
16. Zheng JM, Wu XB, Yang Y (2011) A comparison of preparation method on the electrochemical performances of cathode material $Li[Li_{0.2}Ni_{0.13}Co_{0.13}Mn_{0.54}]O_2$ for lithium ion battery. Electrochim Acta 56:3071–3078
17. Liu JL, Chen L, Hou MY, Wang F, Che RC, Xia YY (2012) General synthesis of $xLi_2MnO_3{\cdot}(1\text{-}x)LiNi_{1/3}Co_{1/3}Mn_{1/3}O_2$ nanomaterials by a molten salt methods: towards a high capacity and high power cathode for rechargeable lithium batteries. J Mater Chem 22: 25380–25387
18. Chen Y, Xu GF, Li JL, Zhang YK, Chen Z, Kang FY (2013) High capacity $0.5\ Li_2MnO_3{\cdot}0.5LiNi_{1/3}Co_{1/3}Mn_{1/3}O_2$ cathode material via a fast co-precipitation method. Electrochim Acta 87:686–692
19. Zhao TL, Chen S, Li L, Zhang XF, Chen RJ, Belharouak I, Wu F, Amine K (2013) Synthesis, characterization, and electrochemistry of cathode material $Li[Li_{0.2}Ni_{0.13}Co_{0.13}Mn_{0.54}]O_2$ using organic chelating agents for lithium-ion batteries. J Power Sources 228:206–213
20. Wang ZY, Liu EZ, He CN, Shi CS, Li JJ, Zhao NQ (2013) Effect of amorphous $FePO_4$ coating on the structure and electrochemical performance of $Li_{1.2}Ni_{0.13}Co_{0.13}Mn_{0.54}O_2$ as cathode material for Li-ion batteries. J Power Sources 236:25–32
21. Jiang KC, Wu XL, Yin YX, Lee JS, Kim J, Guo YG (2012) Superior hybrid cathode material containing lithium-excess layered material and graphene for lithium-ion batteries. ACS Appl Mater Interfaces 4: 4858–4863
22. Wang J, Qiu B, Cao HL, Xia YG, Liu ZP (2012) Electrochemical properties of $0.6Li[Li_{1/3}Mn_{2/3}]O_2$–$0.4LiNi_xMn_yCo_{1-x-y}O_2$ cathode materials for lithium-ion batteries. J Power Sources 218:128–133
23. Zhao C, Kang W, Xue Q, Shen Q (2012) Polymerization-pyrolysis-assisted nanofabrication of solid solution $Li_{1.2}Ni_{0.13}Co_{0.13}Mn_{0.54}O_2$ for lithium-ion battery cathodes. J Nanopart Res 14:1240
24. Tang ZH, Wang ZX, Li XH, Peng WJ (2012) Influence of lithium content on the electrochemical performance of $Li_{1+x}(Mn_{0.533}Ni_{0.233}Co_{0.233})_{1-x}O_2$ cathode materials. J Power Sources 208:237–241
25. Lim JH, Bang HJ, Lee KS, Amine K, Sun YK (2009) Electrochemical characterization of $Li_2MnO_3$-$Li[Ni_{1/3}Co_{1/3}Mn_{1/}$

$_3]O_2$-$LiNiO_2$ cathode synthesized via co-precipitation for lithium secondary batteries. J Power Sources 189:571–575
26. Hashem AM, EI-Taweel RS, Abuzeid HM, Abdel-Ghany AE, Eid AE, Groult H, Mauger A, Julien CM (2012) Structural and electrochemical properties of $LiNi_{1/3}Co_{1/3}Mn_{1/3}O_2$ material prepared by a two-step synthesis via oxalate precursor. Ionics 18:1–9
27. Cho TH, Shiosaki Y, Noguchi H (2006) Preparation and characterization of layered $LiNi_{1/3}Co_{1/3}Mn_{1/3}O_2$ as a cathode material by an oxalate co-precipitation route. J Power Sources 159:1322–1327
28. Lu HQ, Wu F, Su YF, Li N, Chen S, Bao LY (2010) Electrochemical performance of $LiNi_{0.5}Mn_{0.5}O_2$ as cathode material for lithium-ion battery prepared by oxalate co-precipitation route. Acta Phys Chim Sin 26:51–56
29. Han XY, Meng QF, Sun TL, Sun JT (2010) Preparation and electrochemical characterization of single-crystalline spherical $LiNi_{1/3}Co_{1/3}Mn_{1/3}O_2$ powders cathode material for Li-ion batteries. J Power Sources 195:3047–3052
30. Kim HJ, Jung HG, Scrosati B, Sun YK (2012) Synthesis of $Li[Li_{0.19}Ni_{0.16}Co_{0.08}Mn_{0.57}]O_2$ cathode materials with a high volumetric capacity for Li-ion batteries. J Power Sources 203:115–120
31. Wen JW, Zhang DW, Teng YC, Chen CH, Xiong Y (2010) One-step synthesis and improved electrochemical performance of $Li(Ni_{1/3}Co_{1/3}Mn_{1/3})O_2$ by a modified radiated polymer gel method. Electrochim Acta 55:2306–2310
32. Li JF, Xiong SL, Li XW, Qian YT (2012) Spinel $Mn_{1.5}Co_{1.5}O_4$ core-shell microspheres as Li-ion battery anode materials with a long cycle life and high capacity. J Mater Chem 22:23254–23259